PROCEEDINGS OF THE ROYAL SOCIETY A

Proc. R. Soc. A (2006) **462**, 189–209
doi:10.1098/rspa.2005.1572
Published online 9 November 2005

On the indentation of a polymeric membrane

By A. P. S. Selvadurai* and Q. Yu

Department of Civil Engineering and Applied Mechanics, McGill University, 817 Sherbrooke Street West, Montreal, Quebec H3A 2K6, Canada

The paper examines the problem of the transverse indentation of a polymeric membrane that is fixed at its circular boundary. Axisymmetric and asymmetric deformations are induced by axial and off-axis indentation by a rigid indentor with a spherical profile. The mechanical behaviour of the polymeric material is modelled by a constitutive relationship that takes into consideration large strains and viscoplastic strain-rate effects. The results of experimental investigations are compared with predictions of computational modelling of the membrane indentation problem that utilizes a documented finite element code with facilities for user-prescribed constitutive models. It is shown that the computational procedure can accurately model the experimental indentation responses particularly during the loading stage. During unloading stages the trends of the model predictions show a satisfactory correlation.

Keywords: indentation of polymeric membranes; hyperelastic materials; membrane indentation experiments; chemically treated membranes; rate dependency; computational modelling

1. Introduction

In recent years, plasticized poly (vinyl) chlorides (PVCs) have been used as components of engineered barrier schemes developed to prevent migration of contaminants and other hazardous substances from waste sites such as landfill. Despite their extensive usage, the long-term performance and reliability of PVC materials at time-scales relevant to waste containment applications is poorly understood. A PVC liner used as a component of a waste containment barrier can be subjected to a variety of mechanical and environmental effects including loading from accumulating landfill, pressures due to gases entrapped in the landfill and other climatic and environmental factors including solar radiation, corrosive waste, freezing and elevated temperatures generated by exothermic processes in decaying landfill. The goal of this research is to gain a better understanding of the constitutive behaviour of PVC material in its natural state, using a series of transverse indentation tests conducted on an edge-supported PVC membrane. The research also includes the implementation of the constitutive models for the computational evaluation of the response of PVC membranes under various conditions of testing. The specific lateral loading configuration of the PVC membrane involves either an axisymmetric or

* Author for correspondence (patrick.selvadurai@mcgill.ca).

Received 8 March 2005
Accepted 1 September 2005

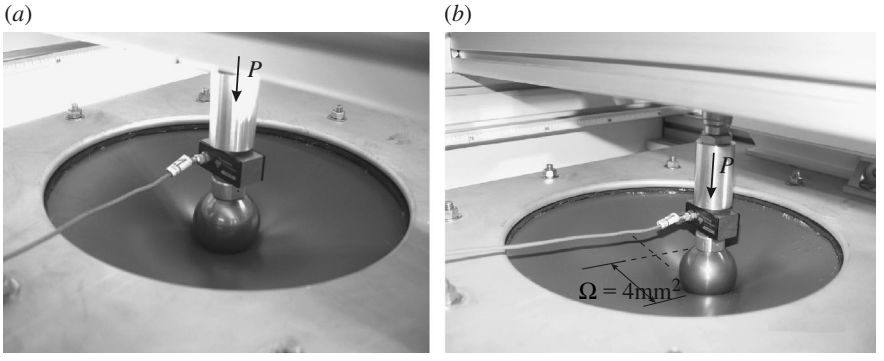

Figure 1. Indentation of a PVC membrane. (*a*) Axisymmetric indentation. (*b*) Asymmetric indentation.

asymmetric indentation through a loaded rigid spherical indentor (figure 1). The problem simulates situations that involve localized loading of membranes in either construction or operation of landfill waste repositories and serves as a useful method for calibrating the constitutive responses of the PVC material, determined from conventional uniaxial testing involving constrained and unconstrained specimens. The indentation test can also give useful information concerning behaviour of a geosynthetic cover liners that may experience ballooning deformations, which can result from the accumulation of gases generated by the decaying waste.

The literature on the mechanics of membranes, in general, is quite extensive and no attempt is made to present a review of all available articles. The history of the study of mechanics of membranes dates back to the work of Föppl, Hencky, Clebsch, Schwerin, Girkmann, von Karman and others and useful historical reviews are given by Timoshenko (1953), Timoshenko & Woinowsky-Krieger (1959) and Naghdi (1972). Many classical studies dealing with the mechanics of membranes focus on the modelling of the large deflection-large rotation response of membranes composed of elastic materials with a linear Hookean response. These include topics such as pressurization and indentation of flat circular membranes comprised of hyper-elastic materials, localized loading of hyper-elastic materials, indentation of membranes with classical elastic constitutive responses, mechanics of membranes with inelastic and time-dependent responses and experimental evaluation of membrane behaviour. A review of literature related to membrane problems associated with hyper-elastic materials is given by Beatty (1987). The recent volume by Libai & Simmonds (1998) also contains a well-documented literature review of membrane problems treated within the context of the nonlinear theory of elastic shells. The applications of nonlinear theories that incorporate time- and rate-effects in the finite strain constitutive responses are not very extensive. The axisymmetric inflation of a nonlinear viscoelastic membrane by lateral pressure was presented by Wineman (1976), while McGuirt & Lianis (1970) used a system of nonlinear Volterra-type integral equations to generate results for the time-dependent constitutive relationship for a vulcanized styrene–butadiene rubber. Feng (1992) considered the time-dependent problem of finite deformation of a membrane with

constitutive response of the nonlinear viscoelastic-type, and presented results of experimental investigations related to the inflation of a plane circular membrane. In addition to the presence of large strain effects, PVC materials also exhibit strain-rate effects and time-dependent responses that are unaccounted for in the conventional hyper-elastic modelling of rubber-like materials (Wang *et al.* 2001; Yu & Selvadurai 2005). The focus of this study is to present the relevant constitutive responses that describe a PVC material and to apply these studies to investigate the behaviour of an edge-supported circular membrane that is subjected to a transverse indentation. In this paper, the constitutive modelling takes into consideration the influence of large strains and both elastic and viscoplastic effects. The constitutive model development mainly utilizes the results of uniaxial tension tests conducted on strip elements of the PVC material at variable strain rates (Selvadurai & Yu 2006). A further uniaxial test that induces non-uniform strains in a stretched specimen is also used for purposes of parameter identification for the constitutive modelling. These constitutive models are implemented in the general-purpose ABAQUS finite element code, to develop computational estimates of the deformations of the PVC membrane with a circular planform, which is subjected to both axisymmetric and asymmetric indentation by a spherical indentor.

2. Constitutive modelling

Pure rubber-like hyper-elastic materials have imperceptible irreversible phenomena in terms of development of permanent deformations and energy dissipation during cycles of loading (Treloar 1943; Rivlin 1948, 1960; Flory 1969; Green & Adkins 1970; Spencer 1970; Ogden 1984; Beatty 1987; Selvadurai 2002). Glassy polymeric materials, such as PVC, exhibit appreciable irreversible effects in the form of development of permanent strains during loading–unloading cycles and are sensitive to strain-rate effects (Arruda *et al.* 1995; Sweeney & Ward 1995). In this paper, we propose a visco-plastic constitutive model to characterize the mechanical response of PVC. This model considers large strain elasticity phenomena, irreversible deformation and strain-rate effects. The results of experiments conducted for constitutive model development are presented by Yu & Selvadurai (2005) and the associated constitutive model development is discussed by Selvadurai & Yu (2006); here we summarize salient features of the model and its capabilities in both duplicating and predicting the uniaxial experimental responses. For the description of the finite deformation we consider a generic particle, the position of which in the reference configuration is denoted by the Cartesian coordinates X_A ($A=1, 2, 3$) and its position in the deformed configuration is denoted by x_i ($i=1, 2, 3$). The deformation gradient tensor is given by

$$\mathsf{F} = \frac{\partial x_i}{\partial X_A}. \tag{2.1}$$

Experimental results indicate that the PVC material is largely incompressible, which requires that, $\det \mathsf{F}=1$. Following the approaches proposed by Kröner (1960) and Lee (1969) for describing the mechanics of continua that undergo finite deformations that exhibit both reversible and irreversible components (see also Owen 1970; Pipkin & Rivlin 1970; Clifton 1972; Miehe 1994; Lubarda 2004;

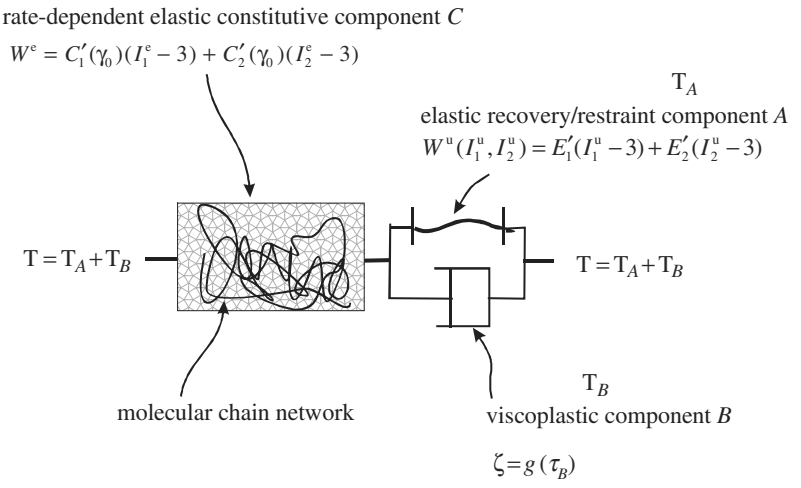

Figure 2. Schematic representation of the constitutive component.

Gurtin & Anand 2005), we assume that the total deformation gradient tensor $\mathbf{F}$ admits a product decomposition into its elastic (e) and irreversible (u) components, i.e.

$$\mathbf{F} = \mathbf{F}^{\mathrm{e}}\mathbf{F}^{\mathrm{u}}. \tag{2.2}$$

Strain tensors in terms of $\mathbf{B}^{\mathrm{e}}$ and $\mathbf{B}^{\mathrm{u}}$ are defined by

$$\mathbf{B}^{\mathrm{e}} = \mathbf{F}^{\mathrm{e}}(\mathbf{F}^{\mathrm{e}})^{\mathrm{T}}, \quad \mathbf{B}^{\mathrm{u}} = \mathbf{F}^{\mathrm{u}}(\mathbf{F}^{\mathrm{u}})^{\mathrm{T}}, \tag{2.3}$$

and the strain rates are defined by (Malvern 1969; Spencer 2004)

$$\boldsymbol{L} = \dot{\mathbf{F}}\mathbf{F}^{-1} = \boldsymbol{D} + \boldsymbol{W} = \dot{\mathbf{F}}^{\mathrm{e}}(\mathbf{F}^{\mathrm{e}})^{-1} + \mathbf{F}^{\mathrm{e}}[\dot{\mathbf{F}}^{\mathrm{u}}(\mathbf{F}^{\mathrm{u}})^{-1}](\mathbf{F}^{\mathrm{e}})^{-1}, \boldsymbol{L}^{\mathrm{u}} = \dot{\mathbf{F}}^{\mathrm{u}}(\mathbf{F}^{\mathrm{u}})^{-1},$$
$$\boldsymbol{D}^{\mathrm{u}} = \frac{1}{2}[\boldsymbol{L}^{\mathrm{u}} + (\boldsymbol{L}^{\mathrm{u}})^{\mathrm{T}}]. \tag{2.4}$$

The invariants of $\mathbf{B}^{\mathrm{e}}$, $\mathbf{B}^{\mathrm{u}}$ are

$$I_1^{\mathrm{h}} = (\lambda_1^{\mathrm{h}})^2 + (\lambda_2^{\mathrm{h}})^2 + (\lambda_3^{\mathrm{h}})^2, \quad I_2^{\mathrm{h}} = \frac{1}{(\lambda_1^{\mathrm{h}})^2} + \frac{1}{(\lambda_2^{\mathrm{h}})^2} + \frac{1}{(\lambda_3^{\mathrm{h}})^2},$$
$$I_3^{\mathrm{h}} = \lambda_1^{\mathrm{h}}\lambda_2^{\mathrm{h}}\lambda_3^{\mathrm{h}} = 1 \quad (\mathrm{h} = \mathrm{e}, \mathrm{u}), \tag{2.5}$$

and λ_i^{e} and λ_i^{u} (i=1, 2, 3) are, respectively, the principal stretches of the elastic and irreversible components. In this paper, the general constitutive model for the PVC material has been selected to conform to a generic form with components as shown in figure 2. The calibration of the results of experimental investigations with a wider class of strain energy functions indicates that the moderately large strain behaviour of the PVC material can be adequately characterized by choosing an internal energy function of the Mooney–Rivlin type (Mooney 1940; Rivlin 1948). The component C of the model (figure 2) is represented by an internal energy function of the Mooney–Rivlin type, and is sufficient to characterize the constitutive behaviour of the PVC material during *monotonic loading* without *unloading*. In this case, there are no irreversible effects and the total deformation gradient $\mathbf{F}$ can be interpreted as an elastic deformation gradient $\mathbf{F}^{\mathrm{e}}$. The stress $\mathbf{T}_C$ associated with the model C, which is the total Cauchy

stress T in the material, is an isotropic function of the elastic strain tensor B^{e} and takes the form

$$\mathsf{T} = \mathsf{T}_C = -\tilde{p}^{\mathrm{e}}\boldsymbol{I} + \psi_1^{\mathrm{e}}\mathsf{B}^{\mathrm{e}} + \psi_2^{\mathrm{e}}(\mathsf{B}^{\mathrm{e}})^2, \quad \psi_1^{\mathrm{e}} = 2\left(\frac{\partial W^{\mathrm{e}}}{\partial I_1^{\mathrm{e}}} + I_1^{\mathrm{e}}\frac{\partial W^{\mathrm{e}}}{\partial I_2^{\mathrm{e}}}\right), \quad \psi_2^{\mathrm{e}} = -2\frac{\partial W^{\mathrm{e}}}{\partial I_2^{\mathrm{e}}}, \tag{2.6}$$

where $\tilde{p}^{\mathrm{e}}$ is a scalar pressure. Following the approach proposed by Sweeney & Ward (1995) to account for the influence of the strain rate on the strain energy function, we adopt the following form of internal energy function for the PVC material

$$W^{\mathrm{e}}(I_1^{\mathrm{e}}, I_2^{\mathrm{e}}) = C_1'(I_1^{\mathrm{e}} - 3) + C_2'(I_2^{\mathrm{e}} - 3), \tag{2.7}$$

where

$$C_1' = C_1 + \begin{cases} \kappa_1 \ln(|\dot{\gamma}_0|/\dot{\gamma}_{\mathrm{c}}) & (|\dot{\gamma}_0| \geq \dot{\gamma}_{\mathrm{c}}), \\ 0 & (|\dot{\gamma}_0| < \dot{\gamma}_{\mathrm{c}}), \end{cases} \quad C_2' = C_2 + \begin{cases} \kappa_2 \ln(|\dot{\gamma}_0|/\dot{\gamma}_{\mathrm{c}}) & (|\dot{\gamma}_0| \geq \dot{\gamma}_{\mathrm{c}}), \\ 0 & (|\dot{\gamma}_0| < \dot{\gamma}_{\mathrm{c}}). \end{cases} \tag{2.8}$$

A detailed account of the thermodynamic basis for introducing the dependency of W^{e} on $\dot{\gamma}_0$ is presented by Selvadurai & Yu (2006). In equation (2.8), $\dot{\gamma}_0$ is a generalized form of a combined stretch rate that depends only on the principal stretches $\bar{\lambda}_i$ $(i=1, 2, 3)$, such that

$$\dot{\gamma}_0 = \frac{\mathrm{d}\gamma_0}{\mathrm{d}t}, \quad \gamma_0 = [(\bar{\lambda}_1 - 1)^{1/\alpha} + (\bar{\lambda}_2 - 1)^{1/\alpha} + (\bar{\lambda}_3 - 1)^{1/\alpha}]^{\alpha}, \tag{2.9}$$

where $\bar{\lambda}_i$ $(i=1, 2, 3)$ have a conditional dependence on the total principal stretches λ_i to take into consideration either the *stretching* or the *unloading* response, i.e.

$$\bar{\lambda}_i = \begin{cases} \lambda_i & (\lambda_i \geq 1), \quad i = (1, 2, 3), \\ 1 & (\lambda_i < 1), \quad i = (1, 2, 3), \end{cases} \tag{2.10}$$

and α is a material parameter that accounts for combined stretch. When a specimen is subjected to a uniaxial stretch, the principal stretches in the lateral directions are less than unity and, therefore, the definition of γ_0 reduces to that of the uniaxial strain ε_0. In equation (2.8), C_1' and C_2' are the modified Mooney–Rivlin-type parameters; κ_1 and κ_2 are parameters that define the strain-rate sensitivity and $\dot{\gamma}_{\mathrm{c}}$ is defined as the *rate-independent threshold strain rate*. With this constraint, at loading rates $|\dot{\gamma}_0| \leq \dot{\gamma}_{\mathrm{c}}$, the strain-rate effects are disregarded. The loading behaviour was studied by examining the stretching behaviour of the uniaxial specimen up to failure at a series of loading rates $\dot{\varepsilon}_0 = 0.4$, 4 and 40% min^{-1}. The relevant material parameters required to define C_1' and C_2' are given by: $C_1 \approx 0.23$ MPa; $C_2 \approx 0.53$ MPa; $\kappa_1 = \kappa_2 = \kappa \approx 0.13$; $\dot{\gamma}_{\mathrm{c}} \approx 5.67 \times 10^{-7}$ s^{-1}. The model representations of the experimental data are presented in figure 3. The results shown in figure 3 corresponding to loading rate $\dot{\varepsilon}_0 = 160\%$ min^{-1} are comparisons between the experimental data and *predictions* derived from the constitutive modelling.

PVC materials will exhibit permanent strains at any level of applied strain. Therefore, an additional visco-plastic model, characterized by an elastic recovery component A in parallel with a visco-plastic component B should be added in series to the component C. Since, the component A accounts for elastic unloading

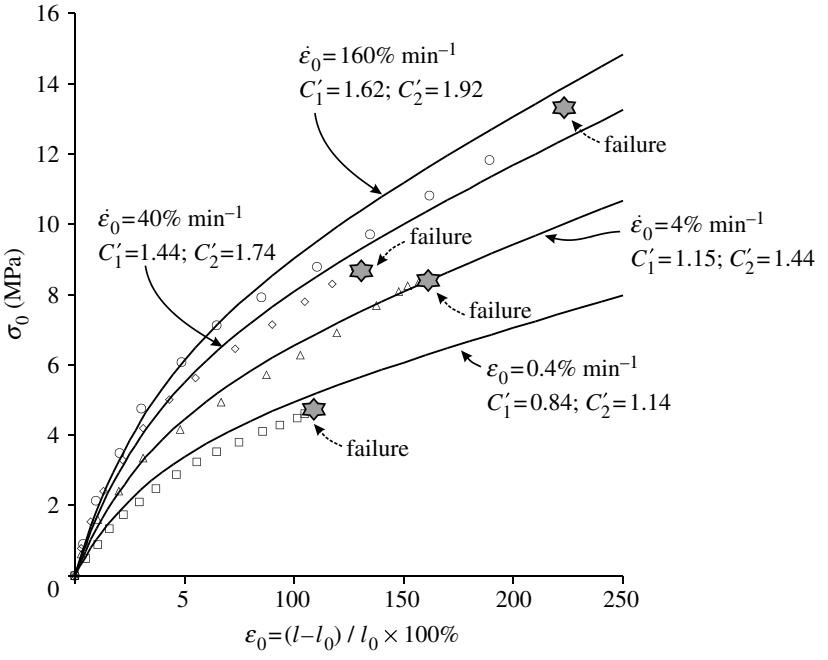

Figure 3. Modelling of the loading part of the uniaxial stress–strain curves (symbols represent experimental data).

at moderately large strains, we can describe the model through the use of an internal energy function of the Mooney–Rivlin form

$$\mathsf{T}_A = -\tilde{p}^{\mathrm{u}}\boldsymbol{I} + \psi_1^{\mathrm{u}}\mathsf{B}^{\mathrm{u}} + \psi_2^{\mathrm{u}}(\mathsf{B}^{\mathrm{u}})^2, \quad \psi_1^{\mathrm{u}} = 2\left(\frac{\partial W^{\mathrm{u}}}{\partial I_1^{\mathrm{u}}} + I_1^{\mathrm{u}}\frac{\partial W^{\mathrm{u}}}{\partial I_2^{\mathrm{u}}}\right), \quad \psi_2^{\mathrm{u}} = -2\frac{\partial W^{\mathrm{u}}}{\partial I_2^{\mathrm{u}}}, \tag{2.11}$$

where $\tilde{p}^{\mathrm{u}}$ is a scalar pressure and

$$W^{\mathrm{u}}(I_1^{\mathrm{u}}, I_2^{\mathrm{u}}) = E_1'(I_1^{\mathrm{u}} - 3) + E_2'(I_2^{\mathrm{u}} - 3). \tag{2.12}$$

In equation (2.12), E_1' is subjected to a conditional constraint, i.e.

$$E_1' = \begin{cases} \to\infty & (\dot{\gamma}_0 \geq -\dot{\gamma}_{\mathrm{c}}^{\mathrm{v}}), \\ 0 & (\dot{\gamma}_0 < -\dot{\gamma}_{\mathrm{c}}^{\mathrm{v}}), \end{cases} \tag{2.13}$$

and E_2' is a constant. The choice of the strain-rate-dependent E_1' in equation (2.12) is intended to take into account the asymmetric behaviour of the elastic recovery component A during the loading–unloading response. The stress T_B in component B is defined in terms of the finite plastic strain rate $\boldsymbol{D}^{\mathrm{u}}$, which is assumed to be related to the deviatoric component of the normalized effective stress tensor N_B. In the component B, the visco-plastic effects are modelled through a relationship of the form (see e.g. Arruda *et al.* 1993; Gurtin & Anand 2005)

$$\boldsymbol{D}^{\mathrm{u}} = \dot{\zeta}\mathsf{N}_B, \quad \mathsf{N}_B = \frac{3}{2\tau_B}\mathsf{T}_B', \quad \tau_B = \left\{\frac{3}{2}\mathrm{tr}[(\mathsf{T}_B')^2]\right\}^{1/2}, \tag{2.14}$$

and $\mathbf{T}'_B$ is the deviatoric component of the Cauchy stress tensor $\mathbf{T}_B$ applicable to visco-plastic phenomena, as depicted in figure 2. Also, in equation (2.14) the visco-plastic strain rate $\dot{\zeta}$ is assumed to be a function of the effective stress τ_B and the strain rate $\dot{\gamma}_0$, i.e.

$$\dot{\zeta} = \left(\frac{\tau_B}{q}\right)^{1-s} |\dot{\gamma}_0| \begin{cases} \dfrac{1}{(|\dot{\gamma}_0|/\dot{\gamma}_c^{\mathrm{v}})^s} & (|\dot{\gamma}_0| \geq \dot{\gamma}_c^{\mathrm{v}}), \\ 1 & (|\dot{\gamma}_0| < \dot{\gamma}_c^{\mathrm{v}}). \end{cases} \tag{2.15}$$

In equation (2.15), s is the *viscous sensitivity* to the strain-rate effect. Also, at extremely low loading rates $|\dot{\gamma}_0| \leq \dot{\gamma}_c^{\mathrm{v}}$, and the dependency of $\dot{\zeta}$ on strain rate $\dot{\gamma}_0$ is neglected; therefore, the parameter q can be interpreted as the *static yielding stress* of the material. It should also be noted that when $s \approx 0$, the value of $\dot{\gamma}_c^{\mathrm{v}}$ is inapplicable and the response of the material reduces to that of a purely plastic material.

Both at the loading stage ($\dot{\gamma}_0 \geq 0$) and at the extremely low loading rates ($|\dot{\gamma}_0| \leq \dot{\gamma}_c^{\mathrm{v}}$) the visco-plastic deformation applicable to the components A and B is constrained by the choice of an infinite value for E'_1. As a result, only the elastic deformation of component C is applicable to the PVC material. Upon unloading, however, the visco-plastic deformation is fully activated due to the zero value of E'_1 chosen in equation (2.13). All three components A, B and C take effect during the unloading of the PVC material. Following Boyce *et al.* (1988), the stress states in the elastic recovery response A (denoted by $\mathbf{T}_A$) and the visco-plastic response B (denoted by $\mathbf{T}_B$) are added to generate the Cauchy stress $\mathbf{T}$, i.e.

$$\mathbf{T} = \mathbf{T}_C = \mathbf{T}_A + \mathbf{T}_B. \tag{2.16}$$

The visco-plastic properties required to model the unloading behaviour of the PVC material can also be determined from the results of uniaxial tests. The experiments were conducted at strain rates of $\dot{\varepsilon}_0 = 4$ and 40% min^{-1} up to a peak strain of 140%, followed by unloading. The specific material parameters applicable for PVC material are as follows: $q \approx 2.0$ MPa; $s \approx 0$; $E'_2 \approx 0.5$ MPa. The model representations of experimental results are shown in figure 4. The results shown in figure 4 at other values of peak strains, $\varepsilon_0 = 60$ and 100% are predictions.

The rate-dependency of PVC material is achieved through $\dot{\gamma}_0$, which further depends on the material parameter α. The results of the uniaxial tests are, however, insufficient to determine this parameter. The effects of this parameter become appreciable particularly when the PVC material experiences a bi-axial stretching. The parameter α was estimated by conducting uniaxial stretching of a square specimen, which is fixed in oblique directions. In this test, the square PVC specimen was fixed along oblique planes inclined at 45° to the axes of loading using a set of aluminium plates and subjected to uniaxial monotonic stretching (figure 5). Although fixity is enforced at certain boundaries of the tested region, at larger strains the material region experiences biaxial effects. This is evident from the distortion of the grid marked on the test specimen. A computational evaluation of the experimental configuration shown in figure 5 is used to determine the parameter α. Since, the elasticity parameters C'_1 and C'_2 have a logarithmic dependence on the combined stretch rate $\dot{\gamma}_0$ (see e.g. equation (2.8)), there is only a marginal sensitivity of the computational results to the parameter α. The correlations between the experimental results and

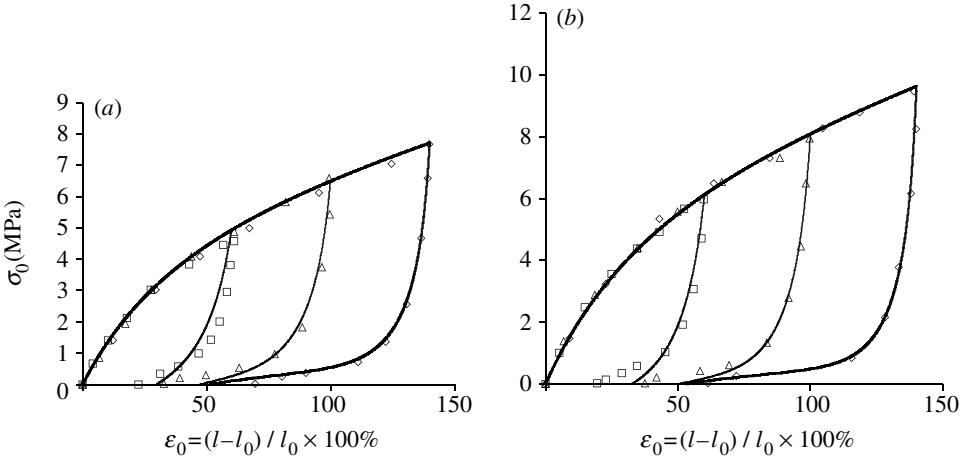

Figure 4. Uniaxial stress–strain curves involving loading and unloading (symbols represent experimental data). (*a*) $\dot{\varepsilon}_0 = 4\%\ \mathrm{min}^{-1}$. (*b*) $\dot{\varepsilon}_0 = 40\%\ \mathrm{min}^{-1}$.

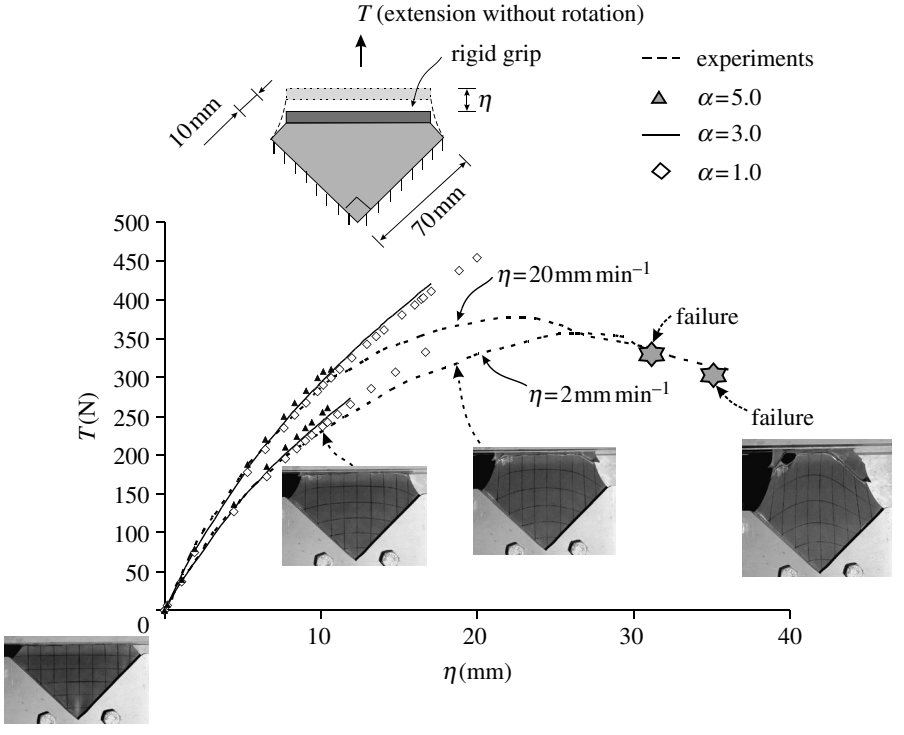

Figure 5. Experimental determination of the material parameter α.

computational modelling were performed with different values of the parameters α conducted at axial stretching rates of $\dot{\eta} = 2$ and 20 mm min^{-1}. At $\eta \leq 7$ mm, which corresponds to a maximum biaxial stretch $\lambda_1 \approx \lambda_2 \approx 1.15$, the computations show only marginal dependence on the value of α. The matching of the computational modelling of the uniaxial test with oblique fixity with the

Table 1. Constitutive equations used for modelling untreated PVC membrane.

components	deformation gradient	component A (T_A)	component B (T_B)	component C (T_C)
loading	$\boldsymbol{F}=\boldsymbol{F}^{\mathrm{e}}$	deformation restricted	deformation restricted	equations (2.6)–(2.10)
unloading	$\boldsymbol{F}=\boldsymbol{F}^{\mathrm{e}}\boldsymbol{F}^{\mathrm{u}}$	equations (2.11) and (2.12) with $E_1'=0$	equations (2.14) and (2.15)	

experimental data can be used for the purposes of identifying the material parameter α. At larger extensions ($\eta>7$ mm), the influence of the parameter α on the computational results is appreciable. The experimental response, however, becomes unreliable due to the slip between the grip and the PVC specimen. Through a comparison between the computational predictions and the experimental results obtained at two extension rates, the parameter α is estimated at a value of 3.0.

In summary, a generalized form of a constitutive model capable of describing large strain hyper-elastic behaviour, strain-rate effects and moderately large irreversible plastic strains has been developed for modelling the mechanical behaviour of a PVC material. The mechanical response, however, has to distinguish between loading and unloading through a selective treatment of the elasticity parameters of the elastic recovery component. During loading, the visco-plastic deformation of the PVC material is restricted and the only deformation is attributed to elastic effects; upon unloading, however, the visco-plastic component is fully activated and unloading behaviour is accompanied by both moderately large elastic strains and irreversible deformations. Table 1 gives a summary of the equations used for describing the general form of the constitutive model for the PVC material during both loading and unloading stress histories.

3. The membrane indentation

(*a*) *Materials*

The thickness (H) of the tested PVC membrane material tested was 0.5 mm, and its major constituent was PVC resin (50–70% weight content). The plasticizer that comprises the major part of the additives accounted for 25–35% of the total weight and transformed the typical brittle PVC polymer to a flexible PVC sheet. The chemical composition of a typical PVC polymer is $(CH_2CHCl)_n$, where n is the number of repeating units.

(*b*) *The test facility*

The membrane indentation apparatus shown in figure 1 was designed to apply a controlled movement to a rigid spherical indentor (with a diameter of 50.8 mm) that interacts with a membrane specimen. The diameter of the plane PVC membrane sample subjected to transverse indentation was approximately 250 mm. The fixed boundary condition was achieved by clamping two aluminium

plates that were secured with 4 mm screws. To reduce the stress concentration near the clamped edge, a rubber sheet of thickness 3 mm, which contained an opening of diameter 250 mm was bonded to the PVC specimen, using non-reactive instant adhesive. During axisymmetric indentation, contact was established at the centre of the membrane (figure 1*a*); indentation was achieved by moving a polished brass indentor (a roughness with maximum asperity difference of 0.2×10^{-6} m) against the membrane at a prescribed constant rate $\dot{\Delta}$. A computer controlled linear actuator was used to move the spherical indentor with a maximum accuracy of 0.025 mm in the displacement. The loads applied to the indentor were low enough to neglect any elastic deformation of both the linear actuator and/or the connecting device. The measurement of the deformed shape of the membrane formed an important component of the experimental results that will be subsequently used in the calibration of the computational predictions. In the current experimental research, attention was restricted to the measurement of the deformed profile using a simplified optical technique. A visual image of the deformed profile was first captured using a high precision (5 Mega pixels) digital camera, mounted 1.5 m from the test specimen. The deflected profiles $w(r)$ and $w(x,0)$ were determined using an image analysis procedure (Klette *et al.* 1998). In this procedure, the physical dimensions of the coordinates, measured in terms of *pixels* in the image plane, were obtained from a calibration against two scales of known dimensions that are located equidistant from the centre of the membrane. The load (P) transmitted through the indentor was measured by a load cell with a peak capacity of 4000 N (1000 lbs). The loads were continuously recorded through a computerized data acquisition system. The indentation response was prescribed through the application of the indentation displacement in an incremental manner up to a maximum displacement of $\Delta_{\max}=76.2$ mm. The ratio of the maximum axial displacement to the membrane diameter reached approximately 0.30 during the axisymmetric loading of the circular PVC membrane. This corresponds to a maximum strain of 40% at the line of separation of contact between the spherical indentor and the PVC membrane. The load–displacement responses for the axisymmetric indentation, shown in figure 6*a*, indicate good repeatability between the sets of experiments. The inset photographic records in figure 6*a* indicate the configuration of the deformed membrane. The PVC material exhibited irreversible deformations after a loading–unloading cycle. During asymmetric indentation, the contacts were initiated at a distance $\Omega=42$ mm from the axis of the circular membrane (figure 1*b*). The maximum indentation displacement applied during the asymmetric indentation was also $\Delta_{\max}=76.2$ mm. This displacement gave rise to a maximum strain of approximately 50% at the line of separation of contact between the spherical indentor and the PVC membrane. In comparison to the case of axisymmetric indentation, larger forces were needed to induce asymmetric indentation (figure 6*b*).

The frictional characteristics between the PVC membrane and the brass indentor can influence the measured indentational load–displacement responses. An independent test was conducted to estimate the frictional properties between the indentor and the PVC membrane under a normal pressure of 6.14 kPa. In these friction experiments, a bronze plate (with maximum asperity difference of approximately 0.5×10^{-6} m) measuring 127×127 mm was allowed to slide on a fixed PVC membrane, at a controlled rate, inducing a relative displacement ϕ at

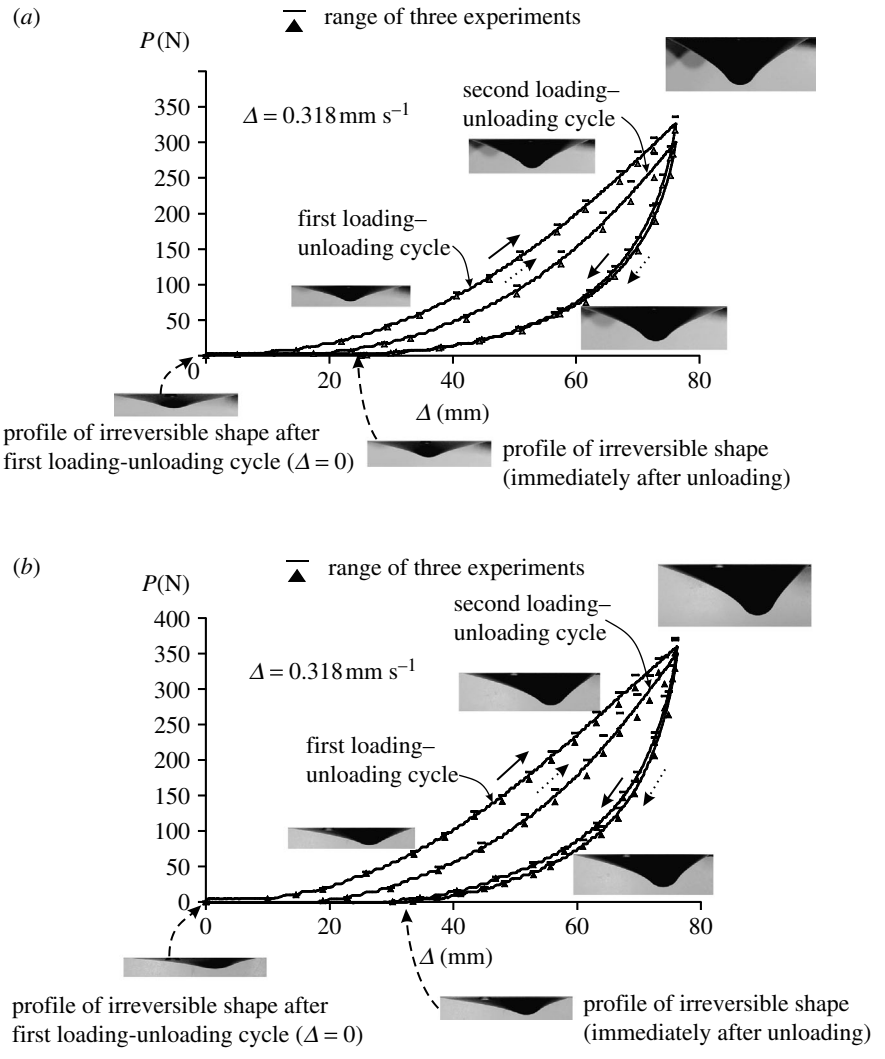

Figure 6. Load–displacement behaviour of the indentor (continuous solid lines correspond to one typical experimental result). (*a*) Axisymmetric indentation. (*b*) Asymmetric indentation.

any given time (figure 7*a*). The preliminary results showed that at the range of velocities of interest, the influence of the relative velocity was negligible. The experiments were then conducted at a velocity of approximately $\dot{\varphi} = 0.5\ \mathrm{mm\ s^{-1}}$, corresponding to the estimated maximum relative velocity between the indenter and PVC membrane achieved during the asymmetric indentation. Considering the relatively low sliding velocities, the inertia effects of the static weight used to induce the normal stress can be neglected. Figure 7*c* shows the variation in the applied friction force with respect to the normalized relative shear displacement. The average value of the coefficient of friction measured during the three sets of tests was 0.52. This normal pressure was, however, much lower than that applied during the indentation (170 kPa for

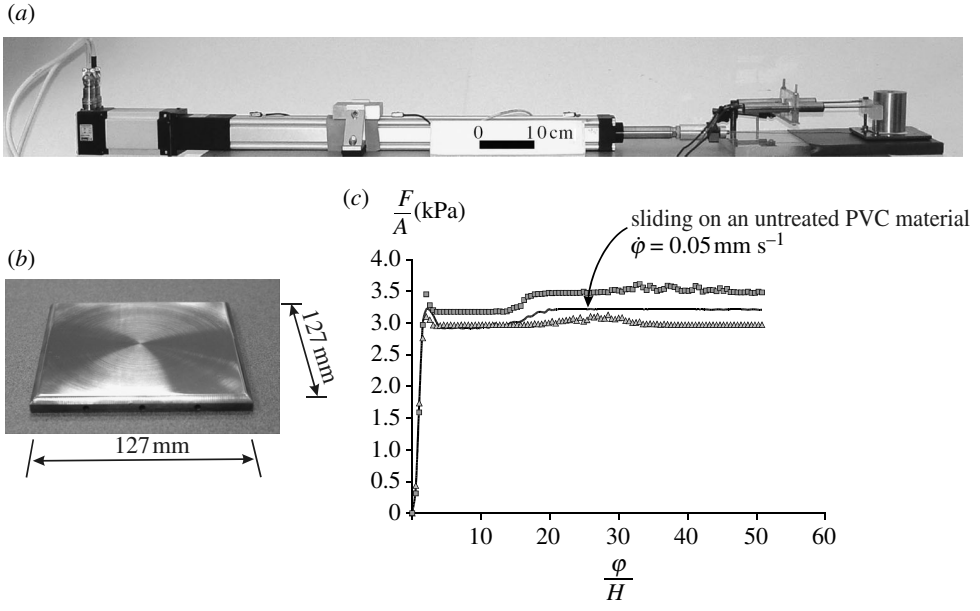

Figure 7. Experimental setup for determining the coefficient of friction between the PVC membrane and the brass plate (ϕ, relative displacement between brass plate and PVC membrane; H, thickness of the PVC membrane). (*a*) Experimental setup. (*b*) Sliding brass plate. (*c*) Experimental results (symbols represent experimental scatter).

axisymmetric indentation and 200 kPa for asymmetric indentation). The work of Schallamach (1953) indicates that the coefficient of friction for rubber-like materials can be influenced by the normal pressure applied at the contact surface. For the purpose of performing the computations, the value of the coefficient of friction is assigned a range of $\mu \in [0.0,0.6]$. The lower limit considers a frictionless contact between the indentor and PVC membrane; and the upper limit is chosen to be approximately 5% higher than that determined from the experiment.

4. Computational implementation

The computational modelling of the indentation of the PVC membrane was performed using the general-purpose finite element code Abaqus (Abaqus/Standard 2004). There are several computational features in Abaqus/Standard that are relevant to the computational modelling of the axisymmetric and asymmetric membrane indentation problem. These include consideration of large strain phenomena, implementation of the contact conditions and, most importantly, the ability to implement the constitutive model derived in §2 in the computational algorithm. Complete descriptions of these procedures are contained in the supplied document in Abaqus/Standard, which is discussed in the User Subroutine UMAT (Abaqus/Standard 2004). In this study, only the last feature will be discussed. In nonlinear analysis performed using Abaqus/Standard code, each step is divided into iteration increments. In this analysis,

we first choose the size of the first displacement increment, and the ABAQUS/Standard code automatically assigns the size of subsequent increments. During each increment, the code employs a Newton–Raphson algorithm to perform the iterations and the equilibrium is determined through consideration of the principle of virtual work, i.e.

$$\int_{V^{\langle t+\Delta t\rangle}} \mathsf{T}^{\langle t+\mathrm{d}t\rangle} : \delta \boldsymbol{D}^{\langle t+\mathrm{d}t\rangle} \mathrm{d}\, V^{\langle t+\mathrm{d}t\rangle} = \int_{S^{\langle t+\Delta t\rangle}} \boldsymbol{t}^{\langle t+\mathrm{d}t\rangle} \cdot \delta \boldsymbol{v}\, \mathrm{d}S^{\langle t+\mathrm{d}t\rangle} + \int_{V^{\langle t+\Delta t\rangle}} \boldsymbol{f}^{\langle t+\mathrm{d}t\rangle} \cdot \delta \boldsymbol{v}\, \mathrm{d}\, V^{\langle t+\mathrm{d}t\rangle}, \tag{4.1}$$

where T is the Cauchy stress; $\delta \boldsymbol{D}$ is the incremental strain rate; $\delta \boldsymbol{v}$ is a vector of virtual displacements; $\boldsymbol{t}$ is a vector of externally applied surface tractions on a unit surface of S; $\boldsymbol{f}$ is a body force vector on a unit volume of V and $\langle t+\mathrm{d}t\rangle$ denotes a state evaluated at time $t+\mathrm{d}t$. For the Newton–Raphson algorithm, we require the Jacobian of the finite element equilibrium equations. The Jacobian, which is obtained by taking the variation of equation (4.1), can be written as

$$\begin{aligned}\int_{V^{\langle t+\mathrm{d}t\rangle}} (\mathrm{d}\mathsf{T}^{\langle t+\mathrm{d}t\rangle} : \delta \boldsymbol{D}^{\langle t+\mathrm{d}t\rangle} + \mathsf{T}^{\langle t+\mathrm{d}t\rangle} : \mathrm{d}\delta \boldsymbol{D}^{\langle t+\mathrm{d}t\rangle}) \mathrm{d}\, V^{\langle t+\mathrm{d}t\rangle} &= \int_{S^{\langle t+\mathrm{d}t\rangle}} \left(\mathrm{d}\boldsymbol{t}^{\langle t+\mathrm{d}t\rangle} \cdot \delta \boldsymbol{v} + \boldsymbol{t}^{\langle t+\mathrm{d}t\rangle} \cdot \delta \boldsymbol{v} \frac{\mathrm{d}A}{A}\right) \mathrm{d}S^{\langle t+\mathrm{d}t\rangle} \\ &\quad + \int_{V^{\langle t+\mathrm{d}t\rangle}} \left(\mathrm{d}\boldsymbol{f}^{\langle t+\mathrm{d}t\rangle} \cdot \delta \boldsymbol{v} + \boldsymbol{f}^{\langle t+\mathrm{d}t\rangle} \cdot \delta \boldsymbol{v} \frac{\mathrm{d}J}{J}\right) \mathrm{d}\, V^{\langle t+\mathrm{d}t\rangle},\end{aligned} \tag{4.2}$$

with

$$A = \frac{\mathrm{d}S^{\langle t+\mathrm{d}t\rangle}}{\mathrm{d}S^{\langle t\rangle}}, \quad J = \frac{\mathrm{d}\, V^{\langle t+\mathrm{d}t\rangle}}{\mathrm{d}\, V^{\langle t\rangle}}, \tag{4.3}$$

where A is the surface area ratio between time $t+\mathrm{d}t$ and t; and J is the volume ratio between time $t+\mathrm{d}t$ and t. The right side of equation (4.2) is defined by the boundary conditions involving the loading conditions and displacement constraints. On the left side, the expressions for the strain measure $\boldsymbol{D}$ and its variations $\mathrm{d}\boldsymbol{D}$ and $\mathrm{d}\delta \boldsymbol{D}$ in terms of the virtual displacement are defined by the displacement interpolation function used in the element definition. It has been shown (ABAQUS/Standard 2004) that the left side of equation (4.2) can be expressed in a more explicit form

$$\int_{V^{\langle t+\mathrm{d}t\rangle}} \Big\{ \mathrm{d}\boldsymbol{D}^{\langle t+\mathrm{d}t\rangle} : \boldsymbol{C}^{\langle t+\mathrm{d}t\rangle} : \delta \boldsymbol{D}^{\langle t+\mathrm{d}t\rangle} - \tfrac{1}{2}\mathsf{T}^{\langle t+\mathrm{d}t\rangle} : [2\boldsymbol{D}^{\langle t+\mathrm{d}t\rangle} \cdot \boldsymbol{D}^{\langle t+\mathrm{d}t\rangle} - (\boldsymbol{L}^{t+\mathrm{d}t})^{\mathrm{T}} \cdot \boldsymbol{L}^{t+\mathrm{d}t}] \Big\} \mathrm{d}\, V^{\langle t+\mathrm{d}t\rangle},$$

where $\boldsymbol{C}$ is the tangential stiffness and a fourth-order tensor defined by

$$\boldsymbol{C} = \frac{\partial(\mathrm{d}\mathsf{T})}{\partial(\mathrm{d}\boldsymbol{D})}. \tag{4.4}$$

The information on both $\boldsymbol{C}$ and T is defined by the constitutive response of the PVC material implemented through the subroutine UMAT available in the ABAQUS/Standard code. The computational procedure used in the code is shown in the flow chart given in figure 8. The ABAQUS/Standard further utilizes

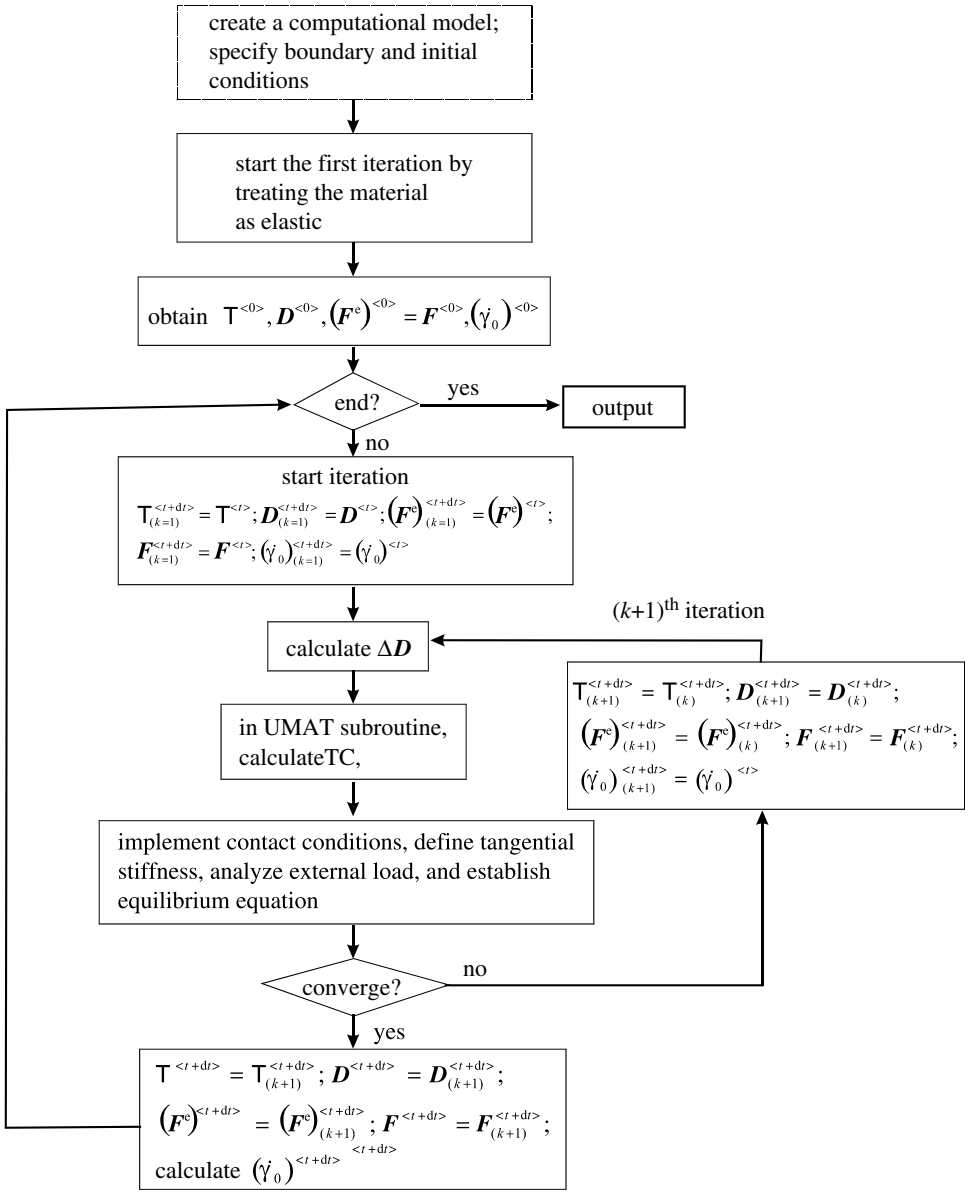

Figure 8. Computational procedures used in Abaqus.

a backward-Euler scheme as a default finite difference scheme to update variables. Those variables that are determined from previous iterations and do not change during the iteration between $[t, t+\mathrm{d}t]$ can be defined as *state variables*. The *state variables* adopted in our analysis include the components of the irreversible deformation gradient F^{u} at time t and the stress tensors at time t in the visco-plastic component including models A and B. When a fully backward-Euler finite difference scheme in time is implemented, the updating of $\dot{\gamma}_0$ requires information on the material configuration at $t+\mathrm{d}t$. The updated

value of $\dot{\gamma}_0$ will further have a direct influence on the elasticity parameters for the element C in the chosen constitutive model, with the result that the computations will exhibit non-convergence. The value of $\dot{\gamma}_0$ is thus assumed to remain unchanged during iteration and is taken as a further *state variable*. For the problems examined here, the PVC membrane only experiences incremental loading during the initial stage where irreversible deformations are absent, the initial values of the state variables can, therefore, be obtained by treating the material as fully elastic. The state variables are updated only when the iteration converges. Both a quadratic triangular membrane element (3M6) and a linear solid triangular prism element (C3D6) were utilized in the computational modelling. The results indicated no noticeable differences between the two types of elements. The computations presented in the paper were developed using the solid triangular prism element.

5. Computational results

The boundary conditions and finite element discretization used in the computational modelling of the axisymmetric transverse indentation of the PVC membrane are illustrated in figure 9*a*. In the case of the axisymmetric indentation problem, a spherical indentor with a rigid surface was configured to move normal to the fixed membrane by achieving contact at the centre of the membrane. For the modelling of contact conditions between the indentor and membrane the *standard hard contact option* in the ABAQUS/Standard code was selected. The computational modelling of the axisymmetric indentation involves the application of a loading rate of $\dot{\Delta} = 0.318\ \mathrm{mm\ s^{-1}}$. The computation first considers a case, where the contact between the indentor and the PVC membrane is frictionless. Figure 10*a* shows the comparison of the load–displacement responses between the computational predictions and experiments during axisymmetric indentation with a loading rate $\dot{\Delta} = 0.318\ \mathrm{mm\ s^{-1}}$. For the purpose of comparison, results are also presented for the unloading mode. The computations slightly underestimate the experimental responses. The computations further consider the case involving a friction coefficient $\mu = 0.6$, which is approximately 5% higher than the value determined from the experiments. As observed both experimentally and computationally, the axisymmetric indentation of the PVC membrane involves almost zero relative slip between the indentor and the PVC membrane. Therefore, the influence of variability in the coefficient of friction on the axisymmetric load–displacement response is marginal. The computations also attempt to correlate the predicted deflected shapes with those determined from the experiments. The computations were performed with the value of a coefficient of friction $\mu = 0.52$, determined from the friction experiments. The computational estimates for the deflected profiles at different loading–unloading stages are presented in figure 11. (The profiles are presented in the x–z plane through the centre of the indentor, which is also parallel to the image plane of the mounted digital camera.) The results presented in figure 11*a* are for three levels of applied load $P = 30$, 150 and 310 N. There is good correlation between the experimental results and the computational estimates. Due to the visco-plastic effects in the polymeric material, the membrane undergoes irreversible deformation after a loading–unloading cycle.

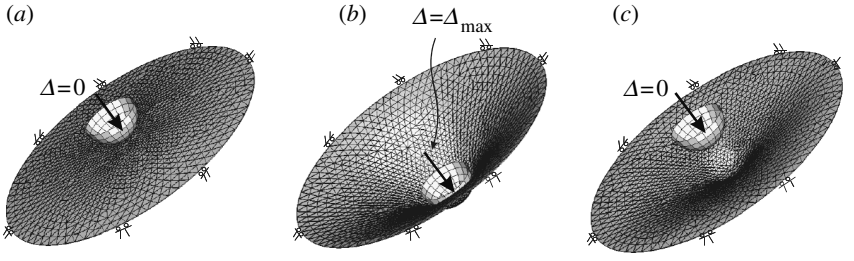

Figure 9. Computational results for axisymmetric indentation of PVC membrane. (*a*) Mesh configuration and boundary conditions (total number of elements: 2086). (*b*) Deformed shape during maximum indentation. (*c*) Irreversible shape after a loading–unloading cycle.

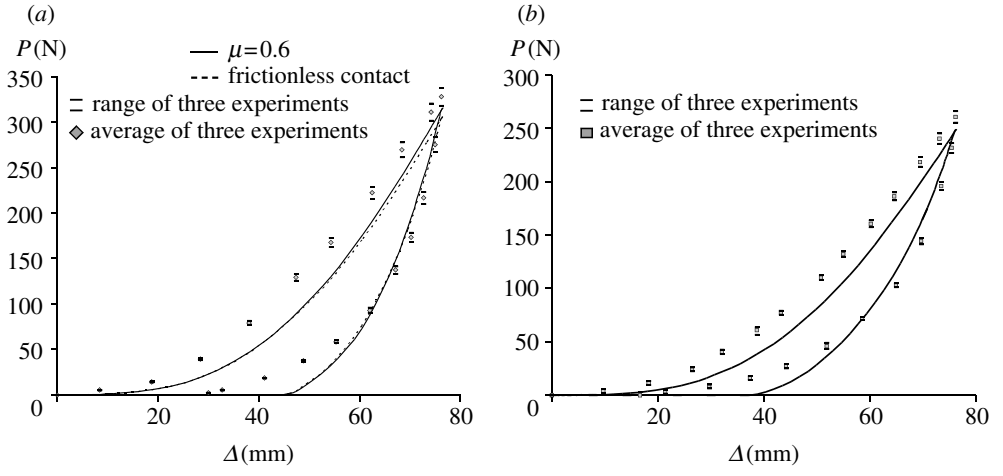

Figure 10. Load–displacement responses of the PVC membrane subjected to axisymmetric indentation (symbols represent experimental data). (*a*) $\dot{\Delta} = 0.318\ \mathrm{mm\ s^{-1}}$, $\mu \in [0.0,0.6]$. (*b*) $\dot{\Delta} = 0.032\ \mathrm{mm\ s^{-1}}$, $\mu = 0.52$.

As a result, the deflection profiles obtained during a loading sequence differ from those determined during an unloading sequence. When the indentation load P reduces to zero after a full loading–unloading cycle, the membrane exhibits a permanent deformation. The computational results tend to overestimate the irreversible deflection during complete release of the applied load. It can be seen that, although the computational results tend to slightly overestimate the experimental results, it gives a reasonably satisfactory prediction of the trend of the load–displacement responses for the unloading paths covering different loading rates. The overestimation of the irreversible deformation is also evident in the uniaxial tests, where the maximum strain is less than 60% (see figure 4*a*,*b*). The maximum strain associated with the axisymmetric indentation is approximately 40%. To obtain a better prediction of the deflected profile during axisymmetric unloading, a more refined constitutive response model needs to be developed for the unloading viscoplastic response model (2.14) particularly for strains in the range of approximately 60%. To further test the predictive

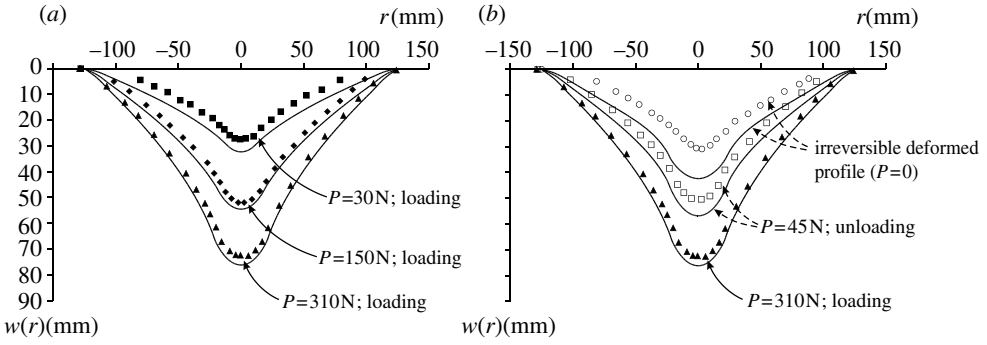

Figure 11. Deflected shapes of PVC membranes during axisymmetric indentation ($\dot{\Delta} = 0.318$ mm s^{-1}; $\mu = 0.52$; symbols represent experimental data). (*a*) During loading. (*b*) During unloading.

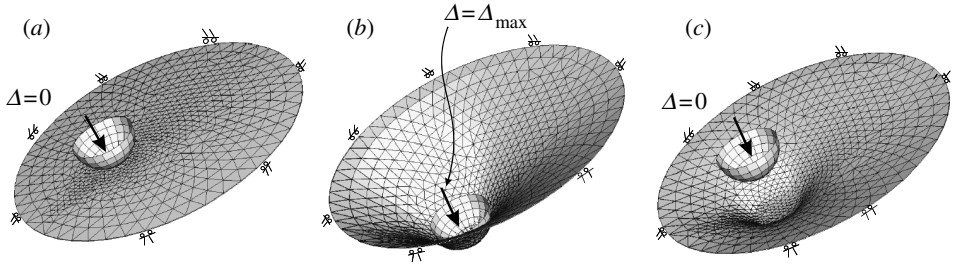

Figure 12. Computational results for asymmetric indentation of PVC membrane. (*a*) Mesh configuration and boundary conditions (total number of elements: 1246). (*b*) Deformed shape during maximum indentation. (*c*) Irreversible shape after a loading–unloading cycle.

capabilities of the computational approach, the problem of the axisymmetric indentation of the membrane at a loading rate of $\dot{\Delta} = 0.032$ mm s^{-1} (which is 10 times lower than the value used previously) was examined (figure 10*b*). The trends of the experimental results correlate well with the computational estimates.

We now focus on the problem of the asymmetric indentation of the polymeric membrane. Figure 12*a* illustrates the boundary conditions and the mesh discretization associated with the membrane indentation problem. In the case of the asymmetric indentation, contact is established at a distance $\Omega = 42$ mm from the centre of the circular membrane at a loading rate of $\dot{\Delta} = 0.318$ mm s^{-1}. The computational modelling first considered the case involving a frictionless contact between the indentor and the PVC membrane (figure 13). The underestimation of the indentation loads by the computational scheme is less significant during the asymmetric indentation. Furthermore, the computational modelling also considers the case involving a much higher coefficient of friction $\mu = 0.6$. The asymmetric indentation of the PVC membrane can involve relative slip between the indentor and PVC membrane; therefore, the influence of a variation in the coefficient of friction was slightly more noticeable in comparison to the results obtained for the modelling involving axisymmetric indentation.

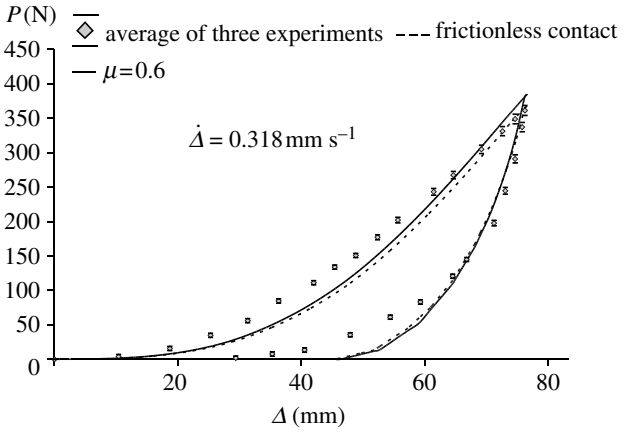

Figure 13. Load–displacement response of the PVC membrane subjected to asymmetric indentation (symbols represent experimental data).

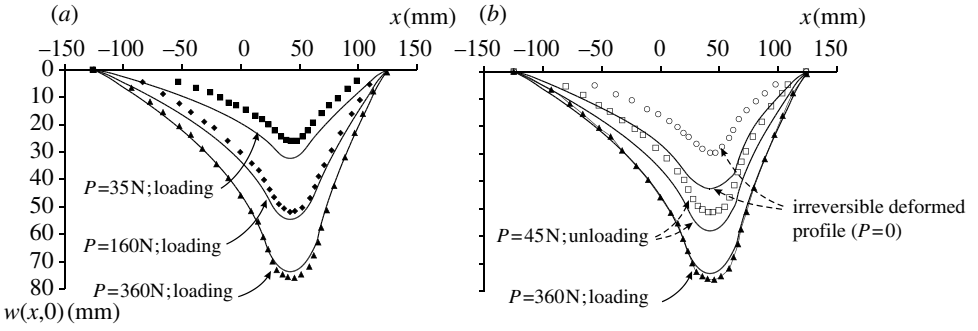

Figure 14. Deflected shape of PVC membrane during asymmetric indentation ($\mu = 0.52$, $\dot{\Delta} = 0.318$ mm s^{-1}; symbols represent experimental data). (*a*) During loading. (*b*) During unloading.

The comparisons between the computed deflected profiles and experimental results are presented for the case involving the friction coefficient $\mu = 0.52$, which is determined from the friction test (figure 14). As with the modelling of the axisymmetric indentation experiment, the computations provide accurate representations for the deflected profiles during the loading stage, but overestimate the irreversible deformation during complete unloading of the membrane. The asymmetric indentation involves a maximum strain of approximately 50%. The overestimation of the irreversible deflection configuration during asymmetric indentation can be attributed to the overestimation of the irreversible deformation during the uniaxial loading that is noticeable at strains less than 60% (see figure 4*a*,*b*).

6. Conclusions

In this paper, an experimentally derived constitutive model, which characterizes the influences of large strains, irreversible deformations and strain-rate

sensitivity of a polymeric PVC membrane, was implemented in the ABAQUS/-Standard finite element code. The computational scheme was used to examine the problem of a flat circular membrane, fixed at its boundary and subjected to both an axisymmetric indentation and an asymmetric indentation. The material parameters in the constitutive model, determined through both uniaxial tensile tests and constrained uniaxial tests were used to predict the mechanical response of an edge-supported circular membrane subjected to transverse indentation. The results show that the computational approach can effectively model the experimental response for indentation at two different loading rates. In the loading mode, the deflected shapes predicted by the computational procedure agree well with the experimental data. An overestimation of the irreversible deformation is, however, observed during the unloading stage. The constitutive parameters contributing to this discrepancy cannot be directly identified through either the material characterization process or through a detailed examination of the indentation profile. The irreversible deformations are largely controlled by the viscoplastic model as defined by the equation (2.14). This model can be further examined and improved to obtain a better correlation between the residual deformations observed in both the uniaxial test data and membrane indentation responses. The overall predictive capabilities of the model are, however, considered to be of value for engineering applications of the constitutive responses for the prediction of the behaviour of PVC membranes under moderately large strains. The success of the methodology adopted here has permitted the application of both the modelling technique and the computational approach for the study of PVC membranes that have been subjected to chemical exposure, which results in both a substantial reduction of the hyper-elastic response and the development of a distinct yield-type phenomenon in the stress–strain response.

The work described in this paper was supported through the *Max Planck Forschungspreis in the Engineering Sciences* awarded by the Max Planck Gesellschaft, Germany and through a *Discovery Grant* of the Natural Sciences and Engineering Research Council of Canada, awarded to the first author. The authors are indebted to a reviewer for the helpful comments.

References

ABAQUS/Standard 2004 *A general-purpose finite element program.* Pawtucket, RI: Hibbitt, Karlsson & Sorensen, Inc.

Arruda, E. M., Boyce, M. C. & Quintus-Bosz, H. 1993 Effects of initial anisotropy on the finite strain deformation behavior of glassy polymers. *Int. J. Plast.* **9**, 783–811. (doi:10.1016/0749-6419(93)90052-R)

Arruda, E. M., Boyce, M. C. & Jayachandran, R. 1995 Effects of strain rate, temperature and thermo-mechanical coupling on the finite strain deformation of glassy polymers. *Mech. Mater.* **19**, 193–212. (doi:10.1016/0167-6636(94)00034-E)

Beatty, M. F. 1987 Topics in finite elasticity: hyperelasticity of rubber, elastomers, and biological tissues—with examples. *Appl. Mech. Rev.* **40**, 1699–1734.

Boyce, M. C., Parks, D. M. & Argon, A. S. 1988 Large inelastic deformation of glassy polymers. Part I. Rate-dependent constitutive model. *Mech. Mater.* **7**, 15–33. (doi:10.1016/0167-6636(88)90003-8)

Clifton, R. J. 1972 On the equivalence of $\mathbf{F}^{e}\mathbf{F}^{p}$ and $\mathbf{F}^{p}\mathbf{F}^{e}$. *J. Appl. Mech., Trans. ASME* **39**, 287–289.

Feng, W. W. 1992 Viscoelastic behavior of elastomeric membranes. *J. Appl. Mech.* **59**, S29–S35.

Flory, P. J. 1969 *Statistical mechanics of chain molecules*. New York: Wiley Interscience.

Green, A. E. & Adkins, J. E. 1970 *Large elastic deformations*, 2nd edn. London: Oxford University Press.

Gurtin, M. E. & Anand, L. 2005 The decomposition $\mathsf{F}=\mathsf{F}^{\mathrm{e}}\mathsf{F}^{\mathrm{p}}$, material symmetry, and plastic irrotationality for solids that are isotropic-viscoplastic or amorphous. *Int. J. Plast.* **21**, 1686–1719. (doi:10.1016/j.ijplas.2004.11.007)

Klette, R., Karsten, S. & Andreas, K. 1998 *Computer vision: three-dimensional data from images*. Singapore: Springer.

Kröner, E. 1960 Allgemeine Kontinuumstheorie der Versetzungen und Eigenspannungen. *Arch. Ration. Mech. Anal.* **4**, 273–334.

Lee, E. H. 1969 Elastic-plastic deformation at finite strains. *J. Appl. Mech., Trans. ASME* **36**, 1–6.

Libai, A. & Simmonds, J. G. 1998 *The nonlinear theory of elastic shells*. Cambridge: Cambridge University Press.

Lubarda, V. A. 2004 Constitutive theories based on the multiplicative decomposition of deformation gradient: thermoelasticity, elastoplasticity, and biomechanics. *Appl. Mech. Rev.* **57**, 95–108. (doi:10.1115/1.1591000)

Malvern, L. E. 1969 *Introduction to the mechanics of a continuous medium*. Upper Saddle River, NJ: Prentice-Hall.

McGuirt, C. W. & Lianis, G. 1970 Constitutive equations for viscoelastic solids. *Trans. Soc. Rheol.* **14**, 117–134. (doi:10.1122/1.549182)

Miehe, C. 1994 On the representation of Prandtl–Reuss tensors within the framework of multiplicative elasto-plasticity. *Int. J. Plast.* **10**, 609–621. (doi:10.1016/0749-6419(94)90025-6)

Mooney, M. 1940 A theory of large elastic deformation. *J. Appl. Phys.* **11**, 583–593. (doi:10.1063/1.1712836)

Naghdi, P. M. 1972 The theory of shells and plates. In *Handbuch der Physik* (ed. S. Flügge & C. Truesdell). Mechanics of solids II, vol. 2, pp. 425–640. Berlin: Springer.

Ogden, R. W. 1984 *Non-linear elastic deformations*. Chichester: Ellis-Horwood.

Owen, D. R. 1970 A mechanical theory of materials with elastic range. *Arch. Ration. Mech. Anal.* **37**, 85–110. (doi:10.1007/BF00281664)

Pipkin, A. C. & Rivlin, R. S. 1970 Mechanics of rate-independent materials. *J. Appl. Math. Phys. (ZAMP)* **16**, 313–327. (doi:10.1007/BF01591911)

Rivlin, R. S. 1948 Large elastic deformations of isotropic materials. IV. Further developments of the general theory. *Phil. Trans. R. Soc. A* **241**, 379–397.

Rivlin, R. S. 1960 Some topics in finite elasticity. In *Structural mechanics* (ed. J. N. Goodier & N. J. Hoff) *Proc. 1st Symp. Naval Structural Mechanics*, pp. 169–198. New York: Pergamon Press.

Schallamach, A. 1953 The velocity and temperature dependence of rubber friction. *Proc. Phys. Soc.* **B66**, 386–392.

Selvadurai, A. P. S. 2002 Second-order elasticity for axisymmetric torsion: a spheroidal coordinate formulation. In *Proc. 2nd Canadian Conf. on Nonlinear Solid Mechanics, Vancouver* (ed. E. Croitoro), vol. 1.

Selvadurai, A. P. S. & Yu, Q. 2006 Constitutive modelling of a polymeric material subjected to chemical exposure. *Int. J. Plast.* (doi:10.1016/j.ijplas.2005.07.005)

Spencer, A. J. M. 1970 The static theory of finite elasticity. *J. Inst. Math. Appl.* **6**, 164–200.

Spencer, A. J. M. 2004 *Continuum mechanics*, 3rd edn. London: Dover Publication.

Sweeney, J. & Ward, I. M. 1995 Rate-dependent and network phenomena in the multi-axial drawing of poly(vinyl chloride). *Polymer* **36**, 299–308. (doi:10.1016/0032-3861(95)91317-Z)

Timoshenko, S. 1953 *History of strength of materials: with a brief account of the history of the theory of elasticity and theory of structures*. New York: McGraw-Hill.

Timoshenko, S. & Woinowsky-Krieger, S. 1959 *Theory of plates and shells*, 2nd edn. New York: McGraw-Hill.

Treloar, L. R. G. 1943 Stress–strain data for vulcanized rubber under various types of deformation. *Trans. Faraday Soc.* **39**, 59–70. (doi:10.1039/tf9433900059)

Wang, Y., Arruda, E. M. & Przybyło, P. A. 2001 Characterization and constitutive modeling of a plasticized poly(vinyl) chloride for a broad range of strain rates. *Rubber Chem. Technol.* **74**, 560–573.

Wineman, A. S. 1976 Large axisymmetric inflation of a nonlinear viscoelastic material by lateral pressure. *Trans. Soc. Rheol.* **20**, 203–225. (doi:10.1122/1.549410)

Yu, Q. & Selvadurai, A. P. S. 2005 Mechanical behaviour of a plasticized PVC subjected to ethanol exposure. *Polym. Degrad. Stab.* **89**, 109–124. (doi:10.1016/j.polymdegradstab.2005.01.007)